Temperature and Strain Rate Dependent Anisotropic Plastic Deformation Behavior of AZ31B Mg Alloy

Aarjoo Jaimin[a], Nitin Kotkunde[a]*, Ayush Morchhale[b], Aditya Raj Anand[a], Anurag Sadhukhan[a], Swadesh Kumar Singh[c,d]

[a] Mechanical Engineering Department, BITS Pilani- Hyderabad Campus, Hyderabad 500 078 India
[b]The Ohio State University 281 W Lane Ave, Columbus, OH 43 210, USA
[c]Mechanical Engineering Department, GRIET, Hyderabad, 500 90 India
[d]Institute for Sustainable Industries & Livable Cities, Victoria University, P.O. Box 14428, Melbourne, VIC 8001, Australia

In the present study, the plastic deformation of commercially available AZ31B alloy at different temperatures (300K-473K) and strain rates ($0.1s^{-1}$-$0.01s^{-1}$-$0.001s^{-1}$) under uniaxial tensile test has been carried out. Three different sheet orientations, viz., rolling direction (RD), transverse direction (TD), and 45° to rolling direction have been used. The outcomes of the experiments have demonstrated a temperature-dependent relationship between mechanical properties such as yield strength, ultimate tensile strength, and percentage elongation. The yield strength and ultimate tensile strength has decreased by 28.58% and 31.03% respectively as temperature increased from 300 K to 473 K. At elevated temperature (473 K) the material has exhibited highest ductility (64.88%) as compare to 300 K. The hardening exponent has been found to decrease with increasing temperature. The flow stress behaviour has been predicted using work hardening models such as the Hollomon and Ludwik. Two-stage work hardening behavior has been observed at all the temperatures. According to statistical parameter comparison, Ludwik equation prediction capability of correlation coefficient (0.9959) has been found to be best in agreement with the experimental results.

1 Introduction

Among various light-weight materials like aluminum and titanium alloys, magnesium alloys have been proven an excellent candidate to achieve high specific strength and low mass density. It has been extensively used in the transportation industries mainly automotive and aerospace domain[1,2]. The major manufacturing challenge of theses alloys are having Hexagonal Closed-Packed (HCP) crystal structure with very limited ductility due to the limited number of slip systems[2]. One of the possible proven solutions is elevated temperature processing which help to improve the ductility and offer ease to fabricate it. One of the essential prerequisite for fabrication of a material is to understand the deformation behavior of a material at different processing conditions[3] G. Mahalle et al.[4] have studied the flow stress behavior of Inconel 718 alloy at elevated temperatures. It has been observed that the yield and ultimate strength decreases with an increase in temperature. Generally, uniaxial tests like tension or compression have extensively used to understand the deformation behavior of a material.

I. Ulacia et al.[5] have performed the tensile tests for AZ31B sheets at various strain rates. Their findings have suggested that the AZ31B alloy showed a hardening behavior with an increment in strain rate. Yi et al.[6] have also analyzed the flow stress behavior from room temperature to 250° C. The mechanical properties like ultimate tensile strength and yield strength have decreased with lower strain rates and higher temperatures. The effect of deformation behavior on maximum stress of AZ31B alloy under compression test at high temperature and low strain rates has studied by Guo et al.[7]. They have found that dynamic recrystallization (DRX) is essential for reducing maximum stress. Ishikawa et al.[8] have successfully investigated the high temperature compressive characteristics of the AZ31 Mg alloy over a wide range of strain rates from 0.001 to 1000 s^{-1}. Their observation has suggested that the deformation mechanism at high strain rates usually proceeds by dislocation glide and twinning even at elevated temperatures. Mukai et al.[9] have also studied the enhancement of ductility in magnesium alloys under dynamic loading.

There are many hardening models, e.g., Hollomon, Ludwik, Swift, and Voce have been used in the

---

*Corresponding author (E-mail:nitink@hyderabad.bits-pilani.ac.in)

analysis of flow behavior of metallic materials. Badrish *et al.*[10] have studied the hot anisotropic tensile flow stress and work hardening behavior for Inconel 625 alloy. A dynamic strain ageing phenomenon has been of room and high temperature. Y. Fu, Y. Cheng, Y. Cui, *et al.*[11] has reported the differential work hardening behavior of AZ31B alloy during uniaxial and biaxial deformation. In the uniaxial loading of hexagonal metals, their findings have revealed only three stages of work hardening. They have mainly interested in the relationship between work hardening and deformation mechanisms. D.T. Nguyen[12] has used Voce's law considering the hardening and softening region in the flow curves separately. The merging of both the equations has efficiently predicted the hardening and softening behavior compared to experimental data. Suh *et al.*[13] have investigated the effect of texture on work hardening behavior. It has been observed the absence of stage II in the K-M plot and maintained that stage III could be effectively analyzed by the differential form of the Voce equation. On the other hand, Y. Koh *et al.* suggested the combined Voce-Swift isotropic hardening law up to UTS for better predictability of the hardening behavior of AZ31B alloy[14]. Thorough studies related to the work hardening behavior of pure magnesium have already been reported[15]. However, due to less symmetry in their crystal structure and complexities associated with plastic deformation, the study of polycrystalline magnesium alloys has always been a challenge to many researchers[16]. Based on a thorough literature review, it has been found that there is indeed a lot of research on AZ31 Mg alloys under various testing conditions. A few studies have reported the influence of plastic behavior through various hardening models. In the present work, the attempt has been made to investigate the anisotropic plastic deformation of AZ31B sheet at different temperatures, strain rates and directions of sheet.

2 Materials and Methods

The Commercially available AZ31B Mg alloy sheets of 1mm thickness were used for the experiment. Table 1 show the chemical composition of the AZ31B Mg alloy. According to the ASTM E8/E011 standard, the sub-size specimens were prepared through a wire-cut EDM process along rolling direction (RD), 45° to RD, and 90° to RD (refer Fig. 1(a&b)).

The specimen's overall length and gauge length were 100 mm and 25 mm, respectively. Uniaxial tensile tests were carried out at 298K, 373 K, 423 K,

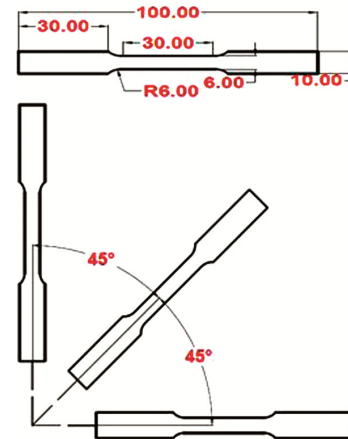| Table 1 — Chemical composition of AZ31B alloy	
Component	wt. %
Mg	96.1
Al	2.67
Zn	0.871
Mn	0.339
Si	0.0466
Fe	0.005
Ni	0.0035
Pb	0.0029
Cu	0.0017
Ca	<0.0001

Fig. 1 — (a) Schematic representation of sub-size specimen used for the uniaxial tensile test (All dimensions are in mm), and (b) Specimen orientations along RD, 45° to RD, & TD.
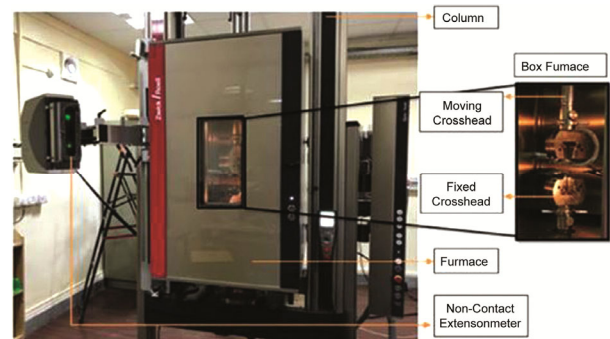

Fig. 2 — Universal Testing Machine (UTM) of 100 KN capacities with non-contact type laser extensometer

and 473 K temperature with three different strain rates (0.1s⁻¹, 0.01s⁻¹, and 0.001s⁻¹) using a Zwick/Roell universal testing machine of 100 KN capacity as shown in Fig. 2. The detailed discussion of experimental set is done by Pandre *et al.*[17] .The test specimens were first heated at 10 °C/min until they reached the deformation temperature, then kept at that temperature for 3 minutes to ensure a homogeneous structure. The true stress-strain response of the specimen was calculated and used for further analysis.
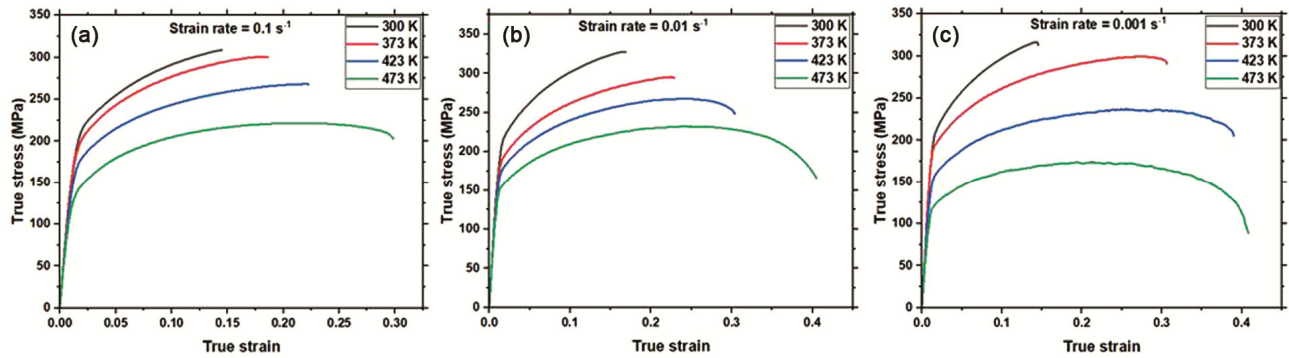
Fig. 3 — Flow stress variation at different temperatures at various strain rates (a) 0.1 s^{-1}, (b) 0.01 s^{-1}, (c) 0.001 s^{-1}
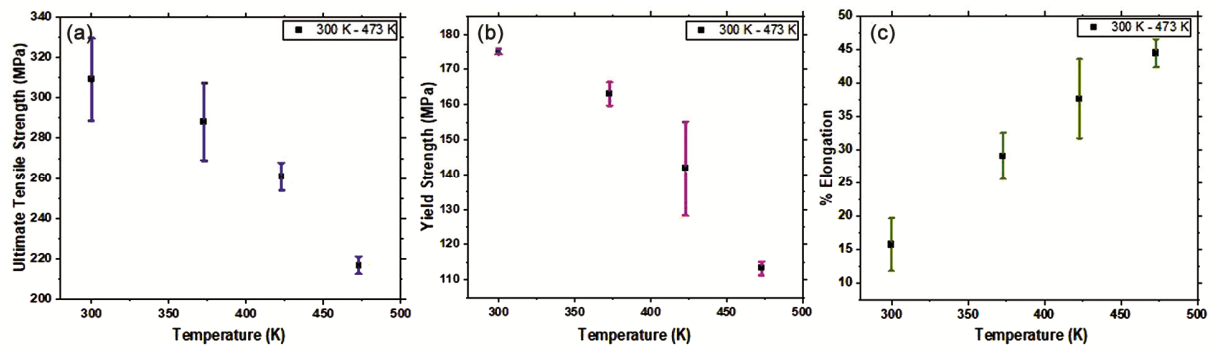

Fig. 4 — Variation of (a) Ultimate stress, (b) Yield stress, and (c) % elongation at different temperatures

3 Results and Discussions

3.1 Flow stress behavior and material properties determination

The true stress-strain curves of the AZ31B magnesium alloy at different temperatures and at particular strain rates were shown in Fig. 3. The flow curve demonstrated strain hardening behavior up to fracture during plastic deformation at ambient temperature. The same pattern may be seen at 373 and 423 K, respectively. At 473 K, a mixture of hardening and softening areas was detected. The strain rate of 0.1 s^{-1} indicated the hardening behaviour till 423 K. The alloy showed a slight thermal softening effect at 423K. as the strain note changed from 0.15^{-1} to 0.0015^{-1}. The softening behaviour was more predominant at 473K for lower strain rate i.e.0.001 s^{-1}.

It was observed from the nature of flow curves that the strength of AZ31B alloy decreased with an increase in temperature. Dislocations can move rapidly; thus, a decrease in strength is reported[13]. One possible reason suggested that with the temperature rise, for pyramidal and prismatic slip systems, critical resolved shear stress (CRSS) decreased in AZ31B magnesium alloy[18]. The non-basal slip systems get activated at higher temperatures, increasing the alloy's ductility. The decrease in flow stress with an increase in temperature and decrease in strain rate can also be explained by the

Table 2 — Calculated mechanical properties of AZ31B alloy at different temperatures

Mechanical properties	Temperature (K)			
	300 K	373 K	423 K	473 K
Yield Strength(MPa)	179.06	162.03	146.27	123.00
Ultimate Tensile Strength(MPa)	310.54	296.18	261.92	221.78
Elongation %	14.21	19.47	25.14	37.64

formation of new dynamically recrystallized (DRX) grains that eliminate substructures[15]. The Table 2 displayed the mechanical properties of AZ31B alloy at different temperatures. The material properties of AZ31B Mg alloy at different strain rates and temperature with orientation as R0 were displayed in Fig. 4. The error bars represented the maximum & minimum experimental values. Ultimate and yield strength of the material were found to be dependent upon temperature as they decreased by an amount of approximately 28.58 % and 31.03 % respectively as temperature increased from 300 K to 473 K.

According to the findings, as the temperature raised, the yield and ultimate tensile strength of the AZ31B alloy decreased significantly. The error bars represented the maximum and minimum experimental values. The strain rate effect can be analyzed by the flow curves depicting different
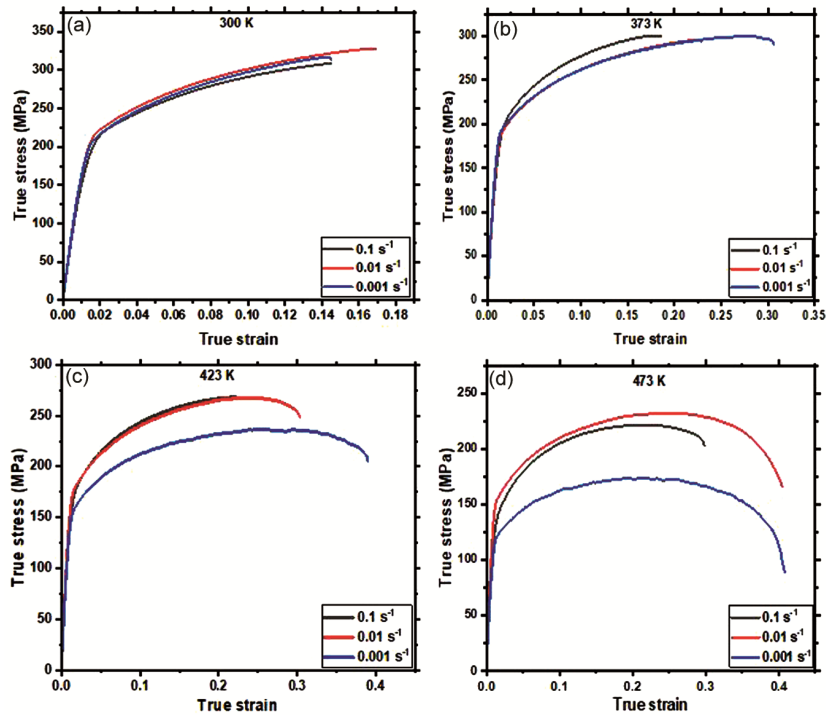
Fig. 5 — Strain rate effect on flow curves at temperatures (a) 300 K, (b) 373 K and (c) 423 K, (d) 473 K

strain rates at constant temperatures as shown in Fig. 5.

The strain rate effect was less significant at room temperature. This effect was predominant at elevated temperatures. The increment in strain rate caused the flow behaviour such as yield and ultimate strength to be reduced but the total elongation to be increased. This observation was due to the accumulation of dislocation density along grain boundaries[7].

The introduction of anisotropy properties in sheet metals was due to various thermo-mechanical treatments, e.g. rolling, extrusion etc. Generally due to this effect, variation in mechanical properties along RD, TD (transverse direction) and 45° to RD was observed.

Uniaxial tensile true stress-strain response of AZ31B with R0, R45, and R90 orientations is depicted in Fig. 6. R45 has the highest ultimate tensile strength, yield strength, and elongation, followed by R0 and R90.

3.2 Strain hardening behavior

The measurement of strain hardening exponent 'n' of any metallic materials can be explained by its capacity to strain hardening during plastic deformation[18].

The 'n' value usually decreases with an increase in temperature for AZ31B alloy. It indicated the temperature and other parameters as depicted
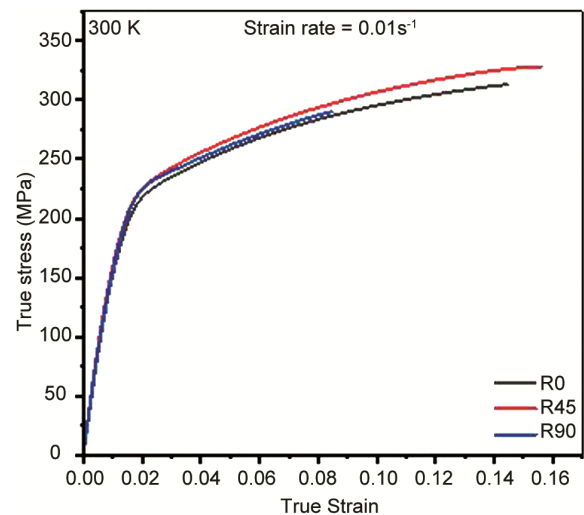

Fig. 6 — Orientation effect on flow curves at 300 K and strain rate 0.01 s^{-1}

nfluence the strain hardening behavior. We need to introduce one term called the Strain hardening capacity (Hc) for better understanding. The hardening capacity of any metallic material can be considered as a ratio of the ultimate tensile strength (σ_{UTS}) to the yield strength (σ_y)[19]. Figure 7(b) showed the variation of Hc at different test temperature the calculated value of hardening capacity at various temperatures is shown in Table 3.
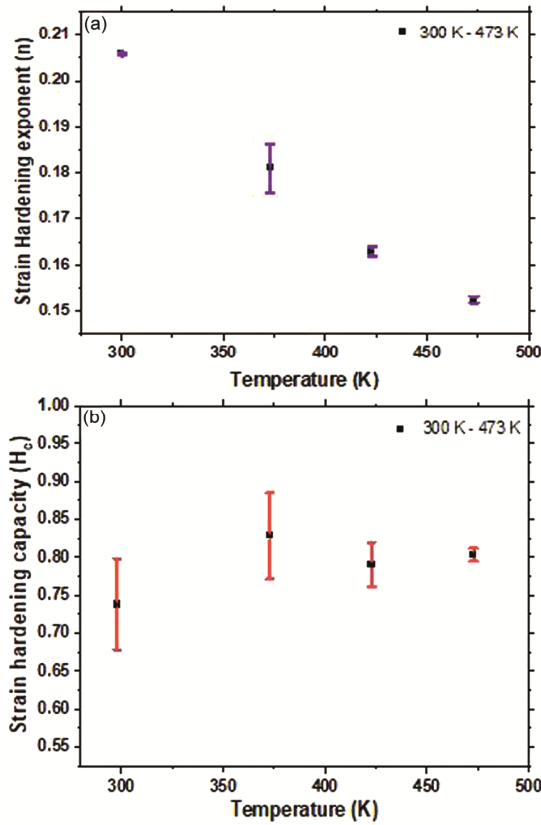
Fig. 7 — Variation of (a) Strain hardening exponent (n) and (b) Strain hardening capacity (H_c) at different test temperatures

Fig. 8 — Hollomon analysis showing 2 stages of strain hardening exponent at different temperatures

Table 3 — Strain hardening exponent values of AZ31B alloy at different temperatures

Temperature (K)	Hardening capacity (H_C)	Hollomon	
		n_{H1}	n_{H2}
300	0.7378	0.5372	0.1917
373	0.8282	0.5353	0.1868
423	0.7904	0.4959	0.1732
473	0.8030	0.3926	0.1813

$$H_c = \frac{\sigma_{UTS} - \sigma_y}{\sigma_y} \qquad \ldots(1)$$

The flow curves and strain hardening behavior of metallic materials has been described using a variety of mathematical relationships. The Hollomon relationship generally expresses the plastic behavior of a material.

$$\sigma = K_H \varepsilon^{n_H} \qquad \ldots(2)$$

Ludwik considered an additional parameter i.e. yield strength in the Hollomon's flow curve equation.

$$\sigma = \sigma_y + K_H \varepsilon^{n_H} \qquad \ldots(3)$$

Where σ is the flow stress, is the yield strength of metallic materials, ε is the plastic strain, n_H is the strain hardening exponent, and K_H is the strength coefficient.
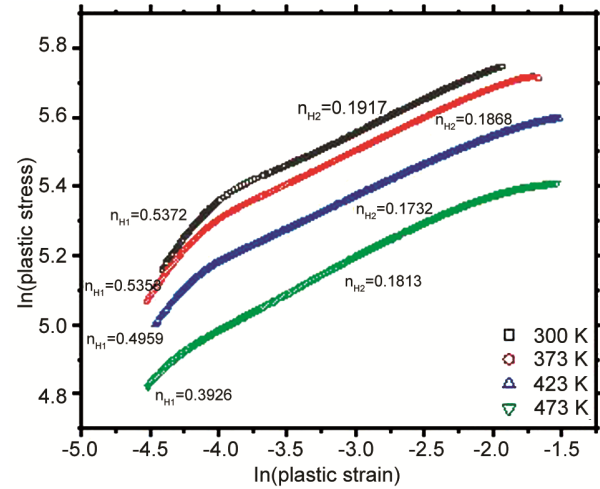
Table 4 — Material parameters for Hollomon and Ludwik at different temperature

Hardening Model	Material Parameters	300 K	373 K	473 K
Hollomon	K_H	470.8	434.5	305.6
	n_H	0.2029	0.1944	0.1805
	R^2	0.9948	0.9938	0.9911
Ludwik	K_L	484.4	386.2	244.8
	n_L	0.6083	0.5211	0.5111
	R^2	0.955	0.9937	0.9959

Determination of hardening exponent (n_H) was done by calculating the slope of the log-log plot for the plastic region at different temperatures. This observation can further be analyzed by two stages of strain hardening. The two different n values were identified in the Hollomon analysis, where n_{H1} and n_{H2} represent the slope of low strain and high strain region, respectively.

From Fig. 8, the slope of the low strain region was higher than the slope of the high strain region for all the temperatures, which indicated the early nH2 strain hardening in AZ31B magnesium alloy at room temperature. With an increase in temperature, the hardening effect decreases gradually.

3.3 Flow curves prediction in hardening region:

The hardening region of AZ31B alloy appeared at room temperature, 373 K and 423 K, respectively, whereas the hardening and softening behavior was observed by 473 K. Hollomon and Ludwik equations were used to predict the flow curves. With the help of experimental data, the material parameters and correlation coefficient (R^2) at various temperatures are shown in Table 4. Hollomon and Ludwik are used to
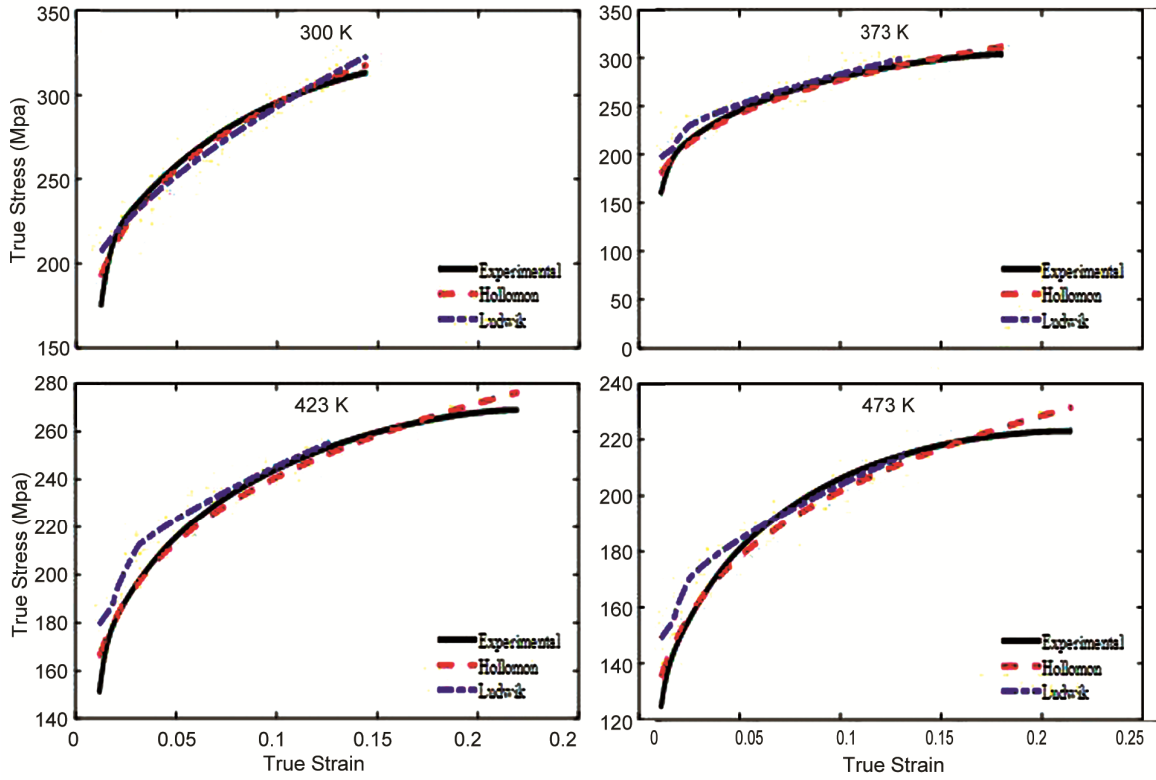
Fig. 9 — Comparison of experimental values and predicted values of Hollomon and Ludwik models at strain rate 0.1 s^{-1} (a) 300 K, (b) 373 K, (c) 423 K, (d) 473 K
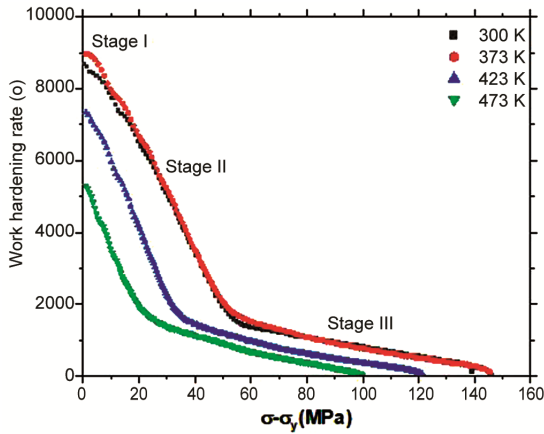

Fig. 10 — K-M plot for work hardening rate and net flow stress

predict the flow curves in the hardening region, as shown in Fig. 9. The Hollomon and Ludwik model displayed excellent correlations for flow stress prediction for temperature ranges from 300 K to 473 K. The deviation from the experiments was predominant for Hollomon at elevated temperatures. In contrast, the Ludwik showed a good correlation of 0.9959 at 473 K. For more clarity, with the help of the Kocks-Mecking (K-M) plot, the stage of deformation under work hardening behavior was determining[20]. The work

hardening rate $\theta = \frac{d\sigma}{d\varepsilon}$ was plotted against the net flow stress $\sigma - \sigma_y$ curves at different temperatures. Generally, three stages of work hardening are observed as illustrated in Fig. 10 in uniaxial loading of hexagonal metallic materials[21].

Stage I refers to an elastic-plastic transition process. In the case of stage II, the work hardening rate is kept almost constant. Linear decrement of work hardening rate is seen in stage III. The slope of stage II is much larger than stage III, and hardening rates decrease linearly with increasing σ-σ$_y$ just after the elastic-plastic transition. From the previous study, the reduction of work hardening rate during stage III may be related to the dynamic recovery originating from cross-slip of <a> dislocations from basal to prismatic planes[22]. For uniaxial loaded AZ31B alloy sheets with strong basal texture, the width strain and thickness strain results from prismatic <a> and pyramidal <c+a>slip[23]. In the uniaxial tensile test at room temperature, the activity of prismatic <a> slip is more significant than pyramidal <c+a> slip, which led to the possible reason for softening behavior of stage III followed by stage I[24].

4 Conclusion

The current study has been based on the uniaxial tensile test at varying temperatures and strain rates and their effect on various mechanical properties. At room temperature, the yield strength (179.06 MPa) and ultimate tensile strength (310.54 MPa) have been lowered to 123 MPa and 221.78 MPa, respectively. At 473 K, the ductility has been improved from 14.21 at room temperature to 37.64 percent.

In addition, the two hardening laws have been established from the true stress-strain data. The stress-strain curves with two stages of hardening have been fitted using the Hollomon and Ludwik equation. A correlation coefficient of 0.9959 at 473 K has been found to be well fitted with the experimental flow stress data for Ludwik equation. A K-M plot is used to investigate the stages in the work hardening behavior of AZ31B alloy. Because of the softening behavior at high temperatures, the slope of stage III has been found be lower than that of stage II.

The Future work will mainly focus on developing various constitutive models and FE analysis.

Acknowledgement

References

1   Yang Q, Xue C, Chu Z, Li Y, Ma L & Gao H, *Scientific Reports*, 11 (2021)17229.
2   Song J, She J, Chen D & Pan F, *J of Mag and Alloys,* 8 (2020) 1.
3   Suh B C, Kim J H, Hwang J H, Shim M S & Kim N J, *Scientific Reports*, 6 (2016) 22364.
4   Mahalle G, Kotkunde N, Gupta A K & Singh S K, *Ad Mat and Proc Tech,* 6 (2020) 456.
5   Ulacia I, Salisbury C P, Hurtado I & Worswick M J, *Mat Proc Tech*, 211 (2011) 830.
6   Khan A, Pandey A, Herold T G & Mishra R K, *Inter J Plast* 27 (2011) 688.
7   Guo Q, Yan H G, Zhang H, Chen Z H & Wang Z F, *Mat Sci and Tech*, 21 (2005) 1349.
8   Ishikawa K, Watanabe H & Mukai T, J Mat Sc, 40 (2005) 1577.
9   Mukai T, Yamanoi M, Watanabe H & Higashi K, Scrip Mater, 45 (2001) 89.
10 Badrish C A, Kotkunde N, Mahalle G, Singh S K & Mahesh K, J Mat Eng Perf 28 (2019) 7537.
11 Fu Y, Cheng Y, Cui Y, Xin Y, Shi S & Chen G, J Mag Alloys, 10 (2022) 478.
12 Nguyen D T, High Temp Mat and Proc, 33 (2014) 499.
13 Suh J, Hernández J V, Letzig D, Golle R & Volk W, Mat Sci Eng A, 650 (2016) 523.
14 Koh Y, Kim D, Seok D Y, Bak J, Kim S W, Lee Y S & Chung K, Inter J Mech Sc, 93 (2015) 204.
15 Nabarro F R N, Basinski Z S & Holt D B, Ad Phy 13 (2006) 193.
16 Koike J, Meta and Mat Trans A, 36 (2005) 1689.
17 Pandre S, Kotkunde N, Takalkar P, Morchhale A, Sujith R & Singh S K, J of Mat Eng and Perf, 28 (2019) 7565.
18 Callister W D & Rethwisch D G, Matsc and eng: An intro 8th Edn ISBN 978-0-470-41997-7.
19 Afrin N, Chen D L, Cao X & Jahazi M, Scrip Materi 57 (2007) 1004.
20 Høgsbro K & Shaw I F, Social Work and Res in Ad Welfare States 1st Edn ISBN 978-0376152185.
21 Valle J A d, Carreño F & Ruano O A, Acta Materi, 54 (2006) 4247.
22 Huang X, Suzuki K, Watazu A, Shigematsu I & Saito N, Mat Sc and Eng A, 488 (2008) 214.
23 Song B, Guo N, Liu T & Yang QS, Mat & Des, 62 (2014) 352.
24 Agnew S R, Tome C N, Brown D W, Holden T M & Vogel S C, Scrip Materi, 48 (2003) 1003.